# Supplementary Information

# for

# MOF dual-purpose with rich S defects cactus like core-shell nanorods MILN-based Co(z)-NiMoS for an efficient electrocatalytic overall water splitting

Honglei Chen[a, b], Zebin Yu*[b], Yanping Hou[b], Ronghua Jiang[c], Jun Huang[d], Wenjun Tang[b], Zhaojun Cao[b], Bo Yang[b], Chunxiang Liu[b], Haonan Song[b]

[a] Guangxi key Laboratory of Electrochemical Energy Materials, Guangxi University, Nanning 530004, P. R. China

[b] School of Resources, Environment and Materials, Guangxi University, Nanning 530004, P. R. China

[c] School of Chemical and Environmental Engineering, Shaoguan University, Shaoguan 512005, P. R. China

[d] College of Civil Engineering and Architecture, Guangxi University, Nanning 530004, P. R. China

* Corresponding author. Tel./fax.: + 8613877108420

## S1. Experiment Section

### S1.1. Synthesis of ZIF-67.

The ZIF-67 was prepared in accordance with previously reported methods. The process was as follows: 0.01 mol $Co(NO_3)_2$ and 0.04 mol 2-methylimidazole were dispersed in 30 mL methanol respectively, and then mixed two solutions quickly and stirred for 24 h at ambient temperature. The product was centrifugated and washed with methanol several times. The obtained purple sample should be kept for 24 h in the vacuum oven at 60 ℃.

### S1.3. Synthesis of 20% Pt/C and $RuO_2$ electrode

Pt/C and $RuO_2$ catalysts were fabricated by methods elaborated elsewhere. In brief, 20 mg of 20 wt.% Pt/C or $RuO_2$ was dissolved in a mixture of 180 μl pure water, 200 μl isopropanol and 20 μl Nafion. That mixture was then ultrasonicated for 1 h to form a homogeneous ink. Subsequently, 40 μl of the ink was loaded onto the NF. Last, the sample was placed in an oven and dried for further testing.

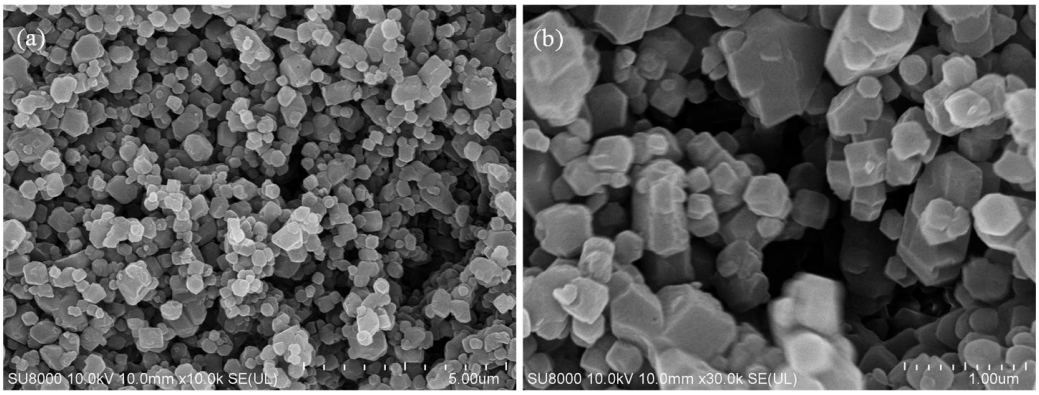


**Fig. S1.** SEM images of ZIF-67.

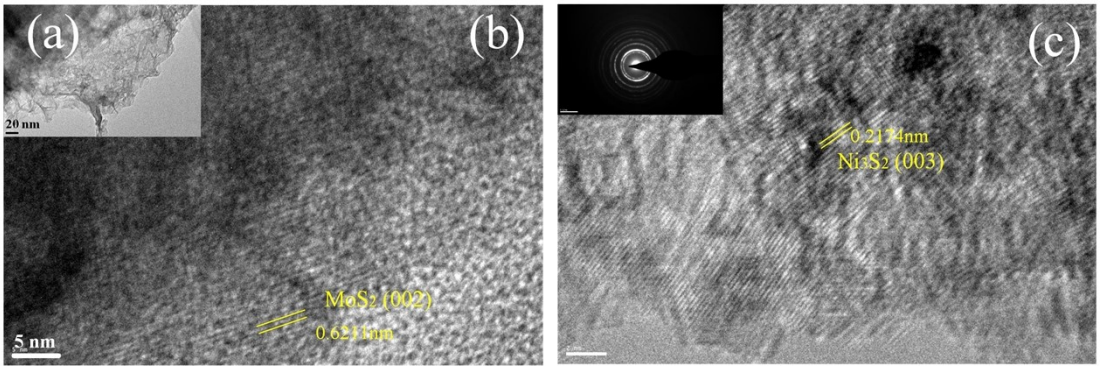


**Fig. S2.** TEM images of NiMoS.

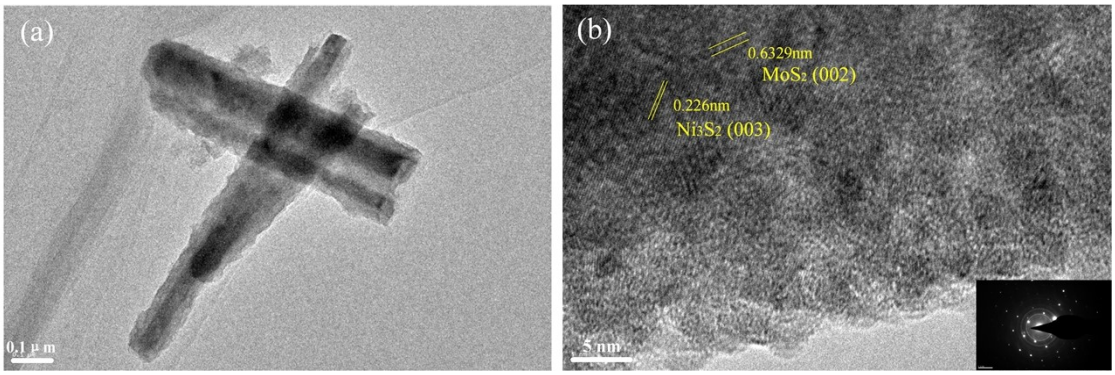


**Fig. S3.** TEM images of Co(z)-NiMoS.

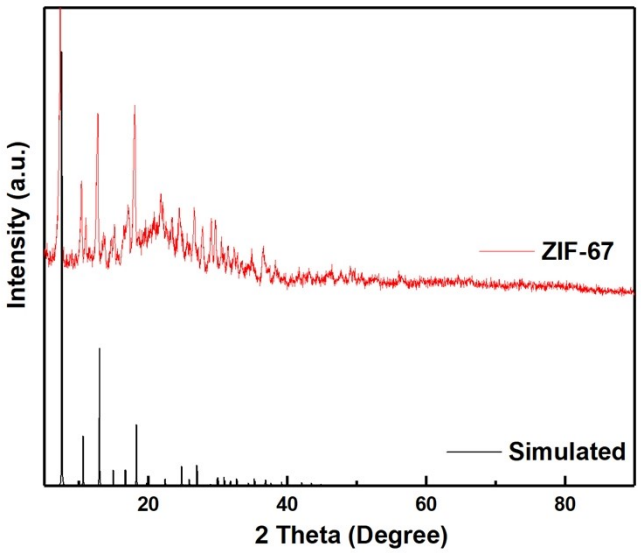


**Fig. S4.** XRD pattern of ZIF-67.

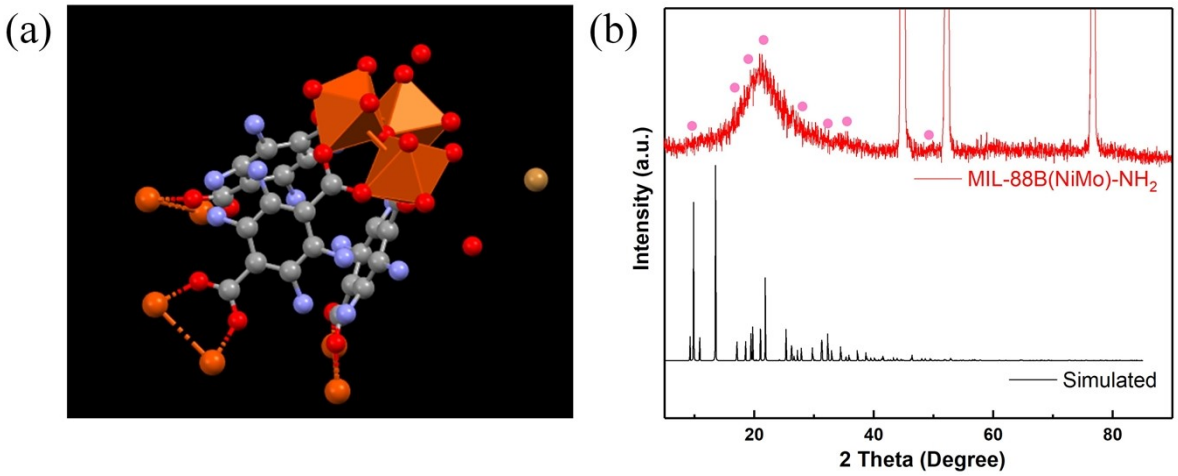


**Fig. S5.** (a) Simulation of atomic structure, (b) XRD pattern of MIL-88B(NiMo)-$NH_2$.

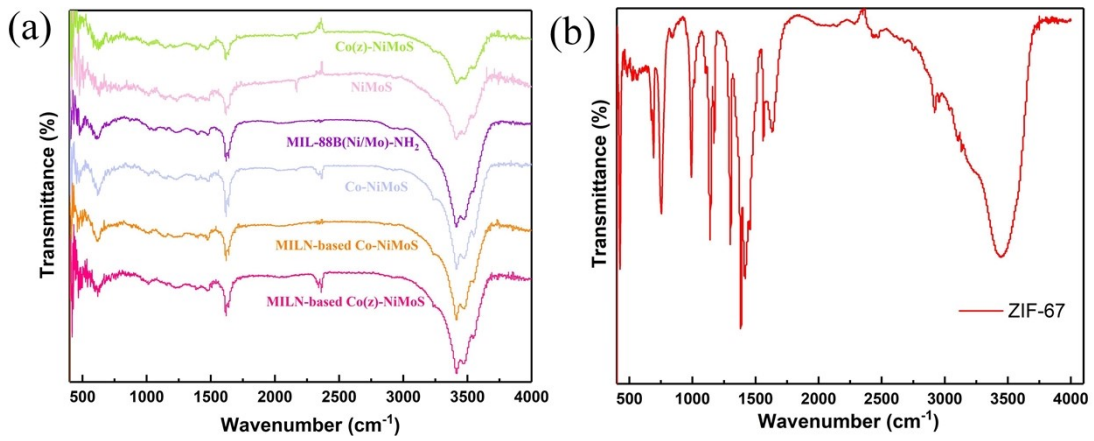


**Fig. S6.** FT-IR spectrum of materials.

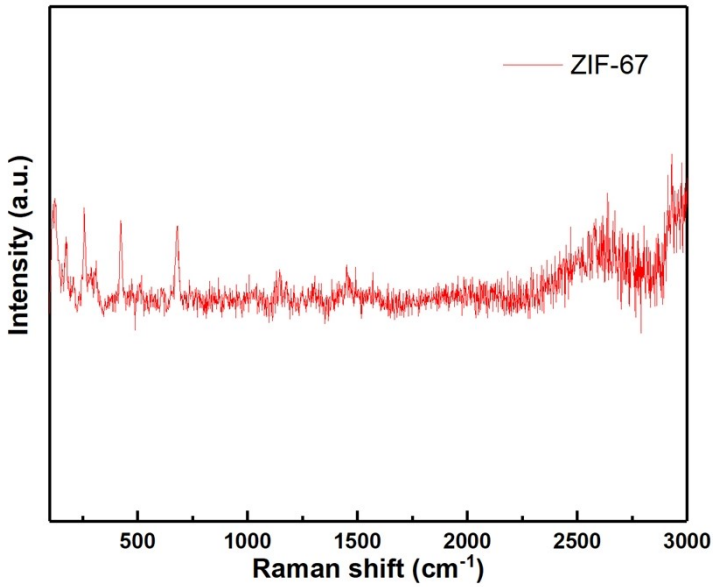


**Fig. S7.** Raman spectrum of ZIF-67.

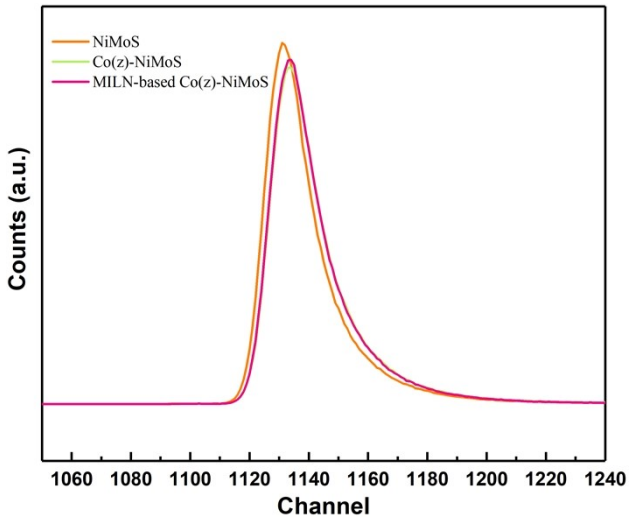


**Fig. S8 Positron lifetime spectra of NiMoS, Co(z)-NiMoS and MILN-based Co(z)-NiMoS.**

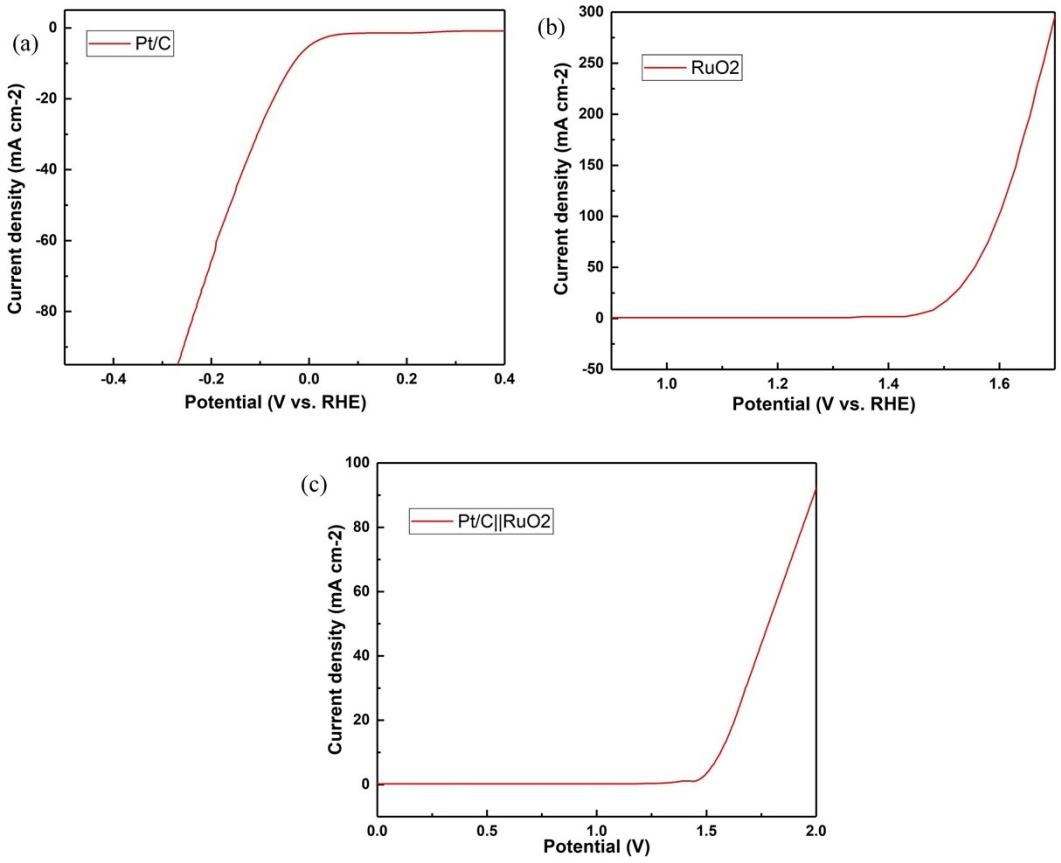


**Fig. S9.** IR-compensation LSV curves of (a) commercial Pt/C, (b) commercial $RuO_2$ and (c) two-electrode formed by commercial Pt/C and commercial $RuO_2$.

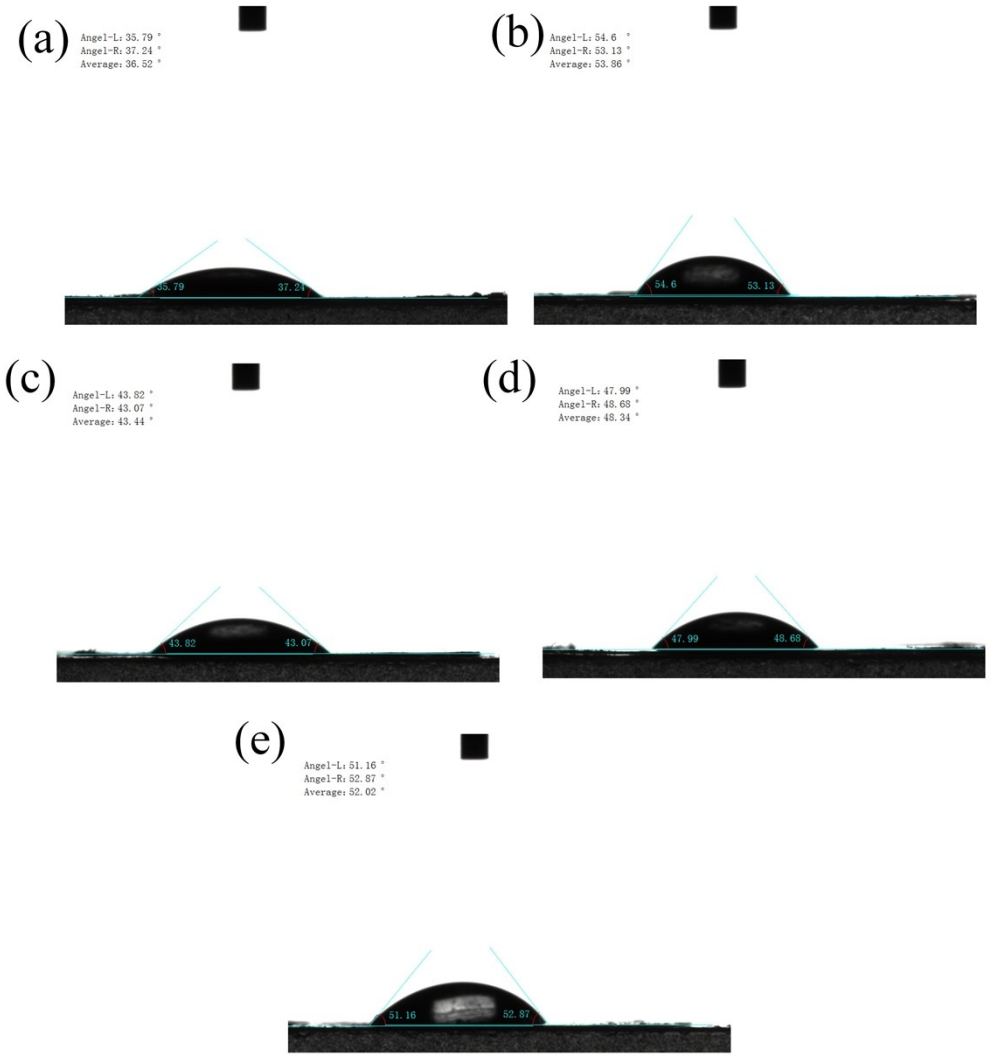


**Fig. S10.** Contact angle measurement of (a) MILN-based Co(z)-NiMoS, (b) NiMoS, (c) Co(z)-NiMoS, (d) Co-NiMoS and (e) MILN-based Co-NiMoS.

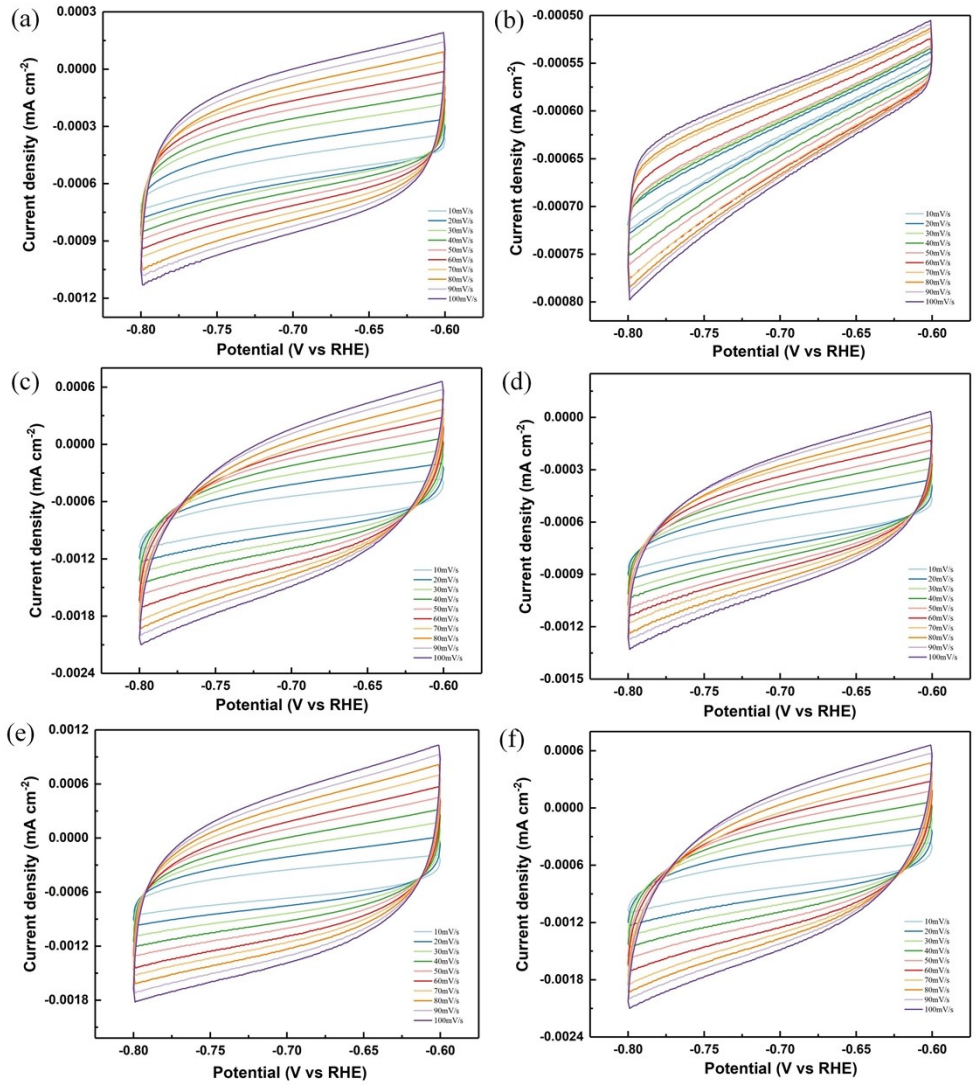


**Fig. S11.** CV curves of the prepared of different samples. (a) MILN-based Co(z)-NiMoS, (b) MIL-88B(Ni/Mo)-$NH_2$, (c)NiMoS, (d)Co(z)-NiMoS, (e) Co-NiMoS (f) MILN-based Co-NiMoS. the corresponding CVs measured at different scan rates from 10 to 100 mV $s^{-1}$ current density at -0.70 V (vs. RHE) was plotted vs. scan rate.

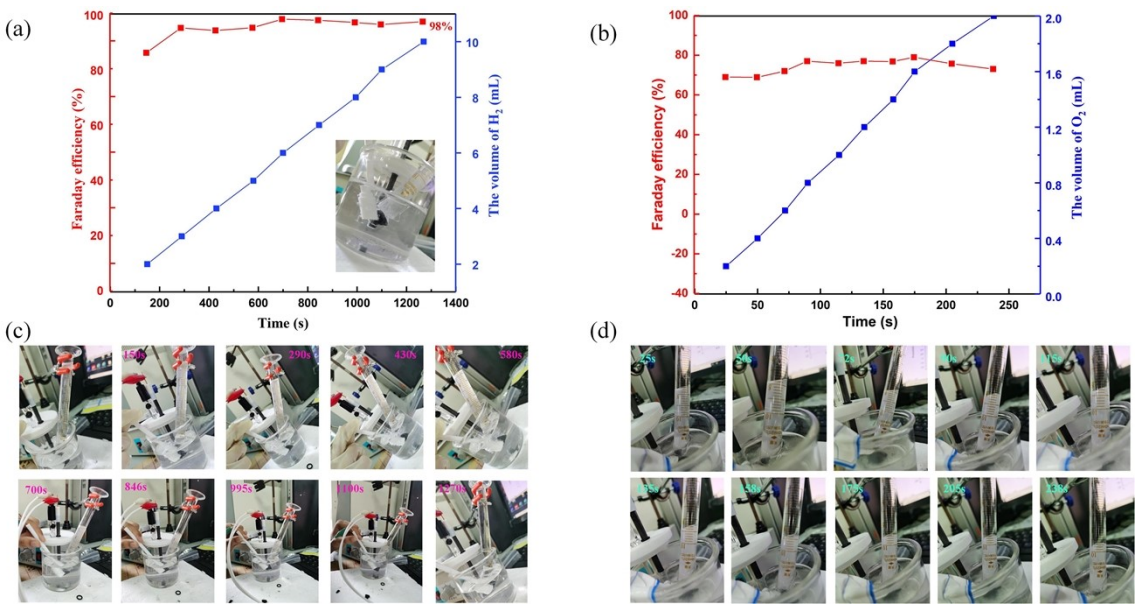


**Fig. S12.** (a) Faraday efficiency and the volume of $H_2$ of the MILN-based Co(z)-NiMoS for HER at various reaction time and photograph of Faraday efficiency test, (b) Faraday efficiency and the volume of $O_2$ of the MILN-based Co(z)-NiMoS for OER at various reaction time, (c-d) Photographs of $H_2$ and $O_2$ collected at various reaction times.

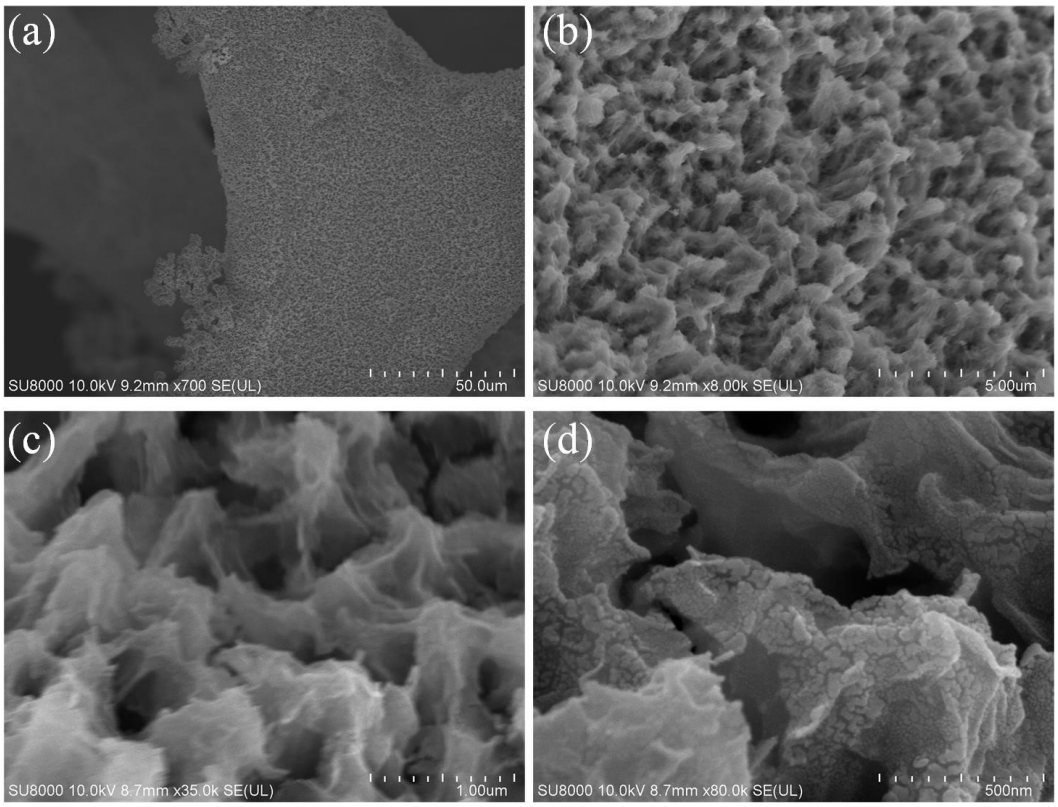


**Fig. S13.** SEM images of MILN-based Co(z)-NiMoS after HER stability test.

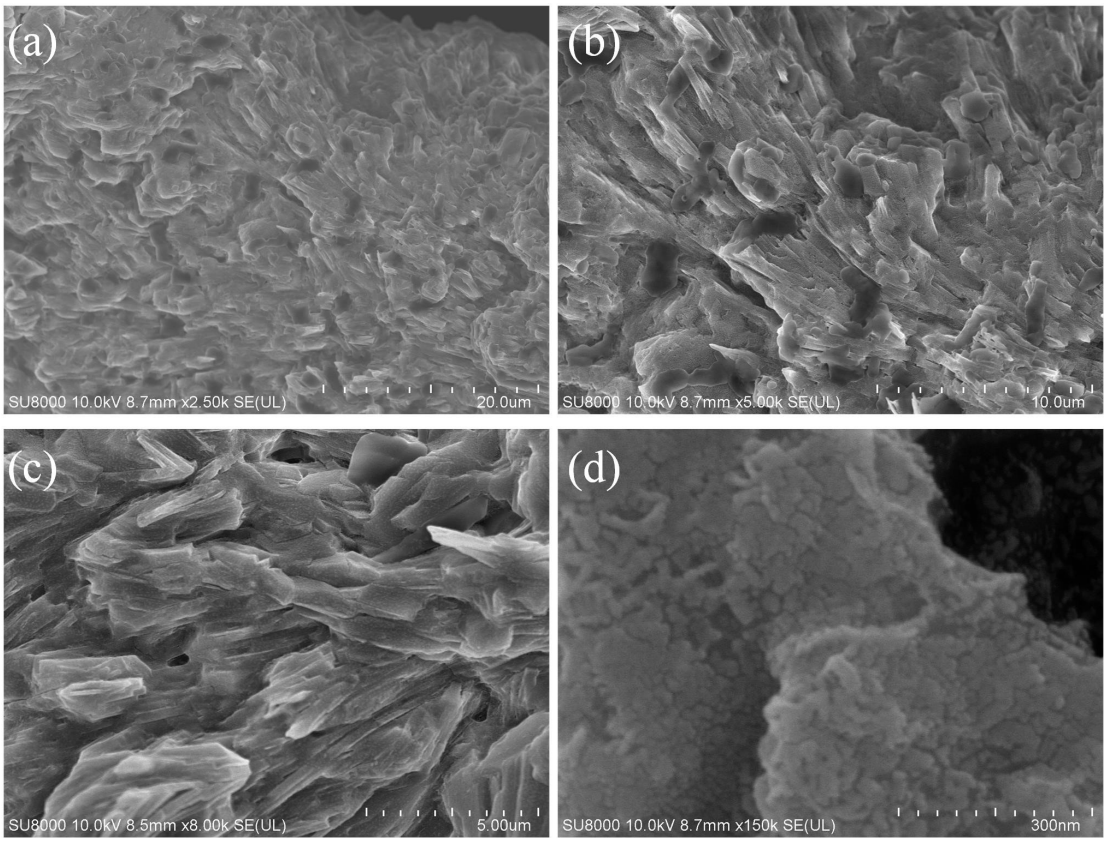


**Fig. S14.** SEM images of MILN-based Co(z)-NiMoS after OER stability test.

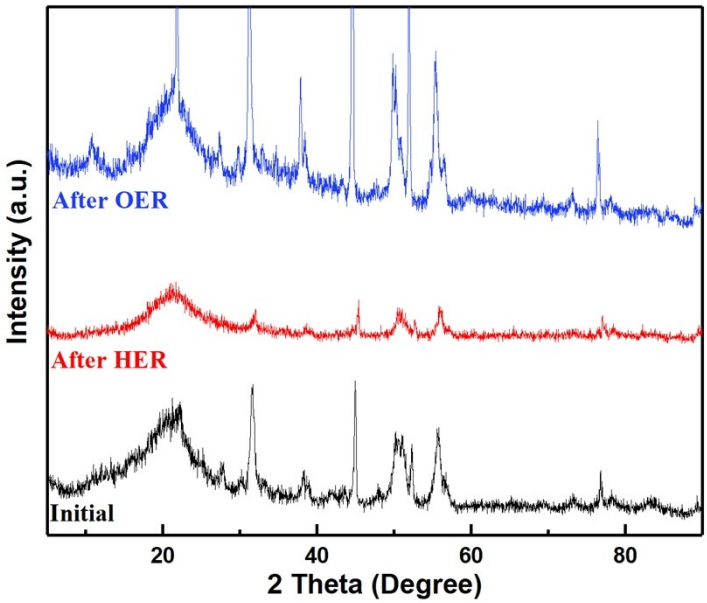


**Fig. S15.** XRD pattern of MILN-based Co(z)-NiMoS before and after stability test.

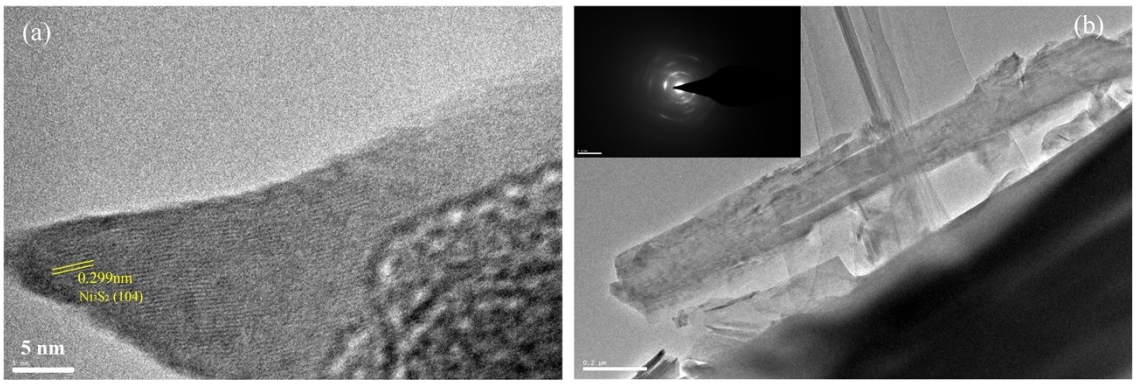


**Fig. S16.** TEM images of MILN-based Co(z)-NiMoS after HER stability test.

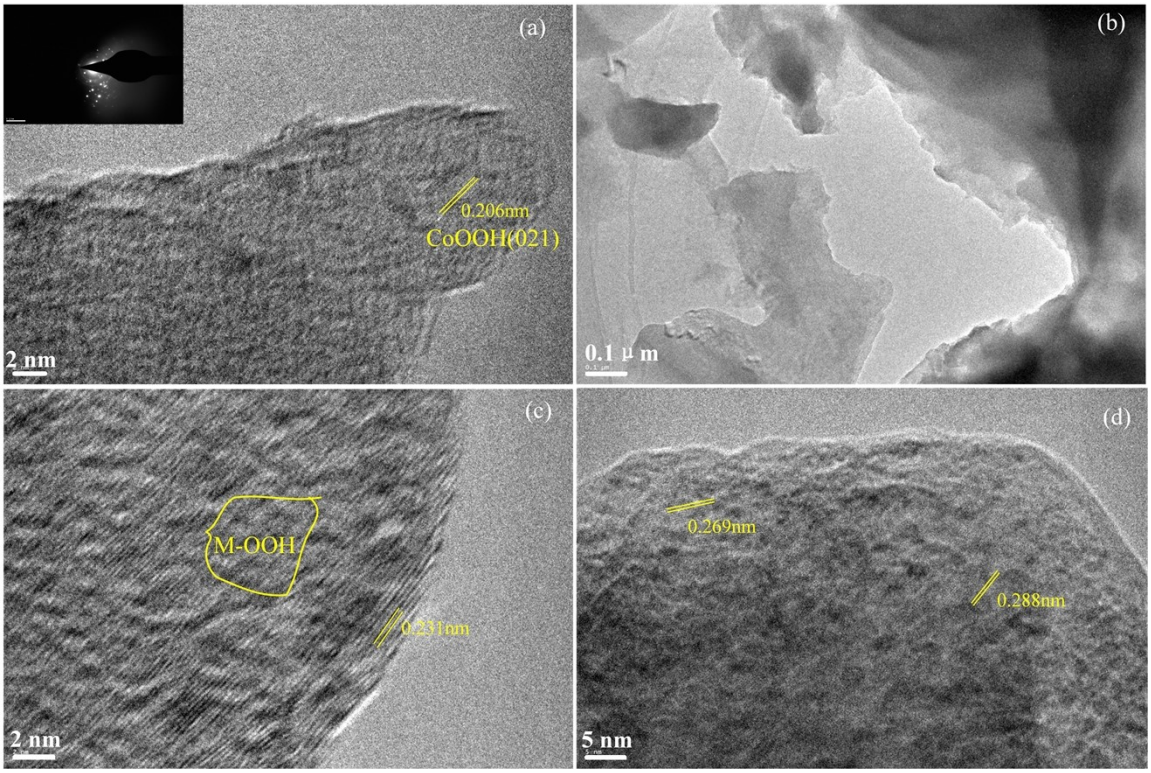


**Fig. S17.** TEM images of MILN-based Co(z)-NiMoS after OER stability test.

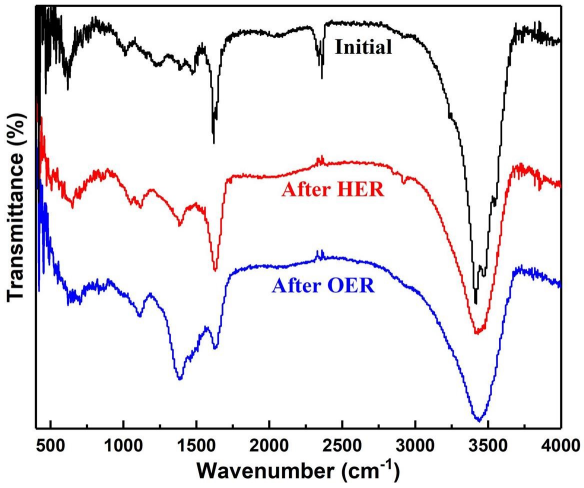


**Fig. S18.** FT-IR spectrum of MILN-based Co(z)-NiMoS before and after stability test.

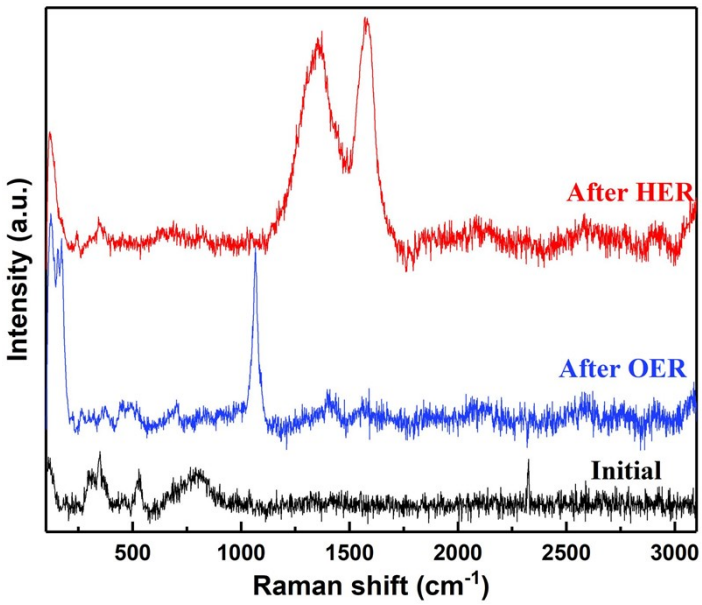


**Fig. S19.** Raman spectrum of MILN-based Co(z)-NiMoS before and after stability test.

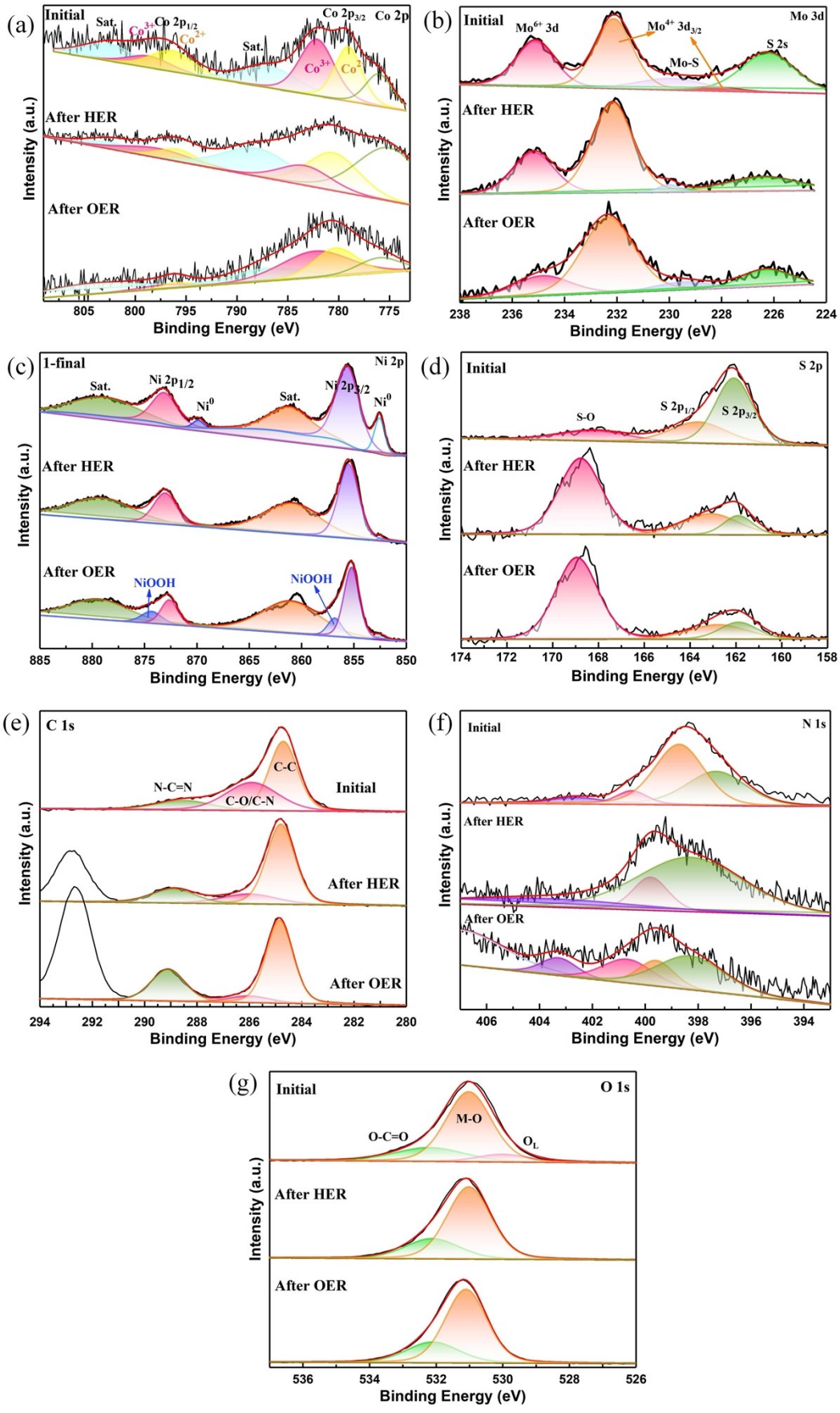


**Fig. S20.** XPS spectra of MILN-based Co(z)-NiMoS before and after stability test.

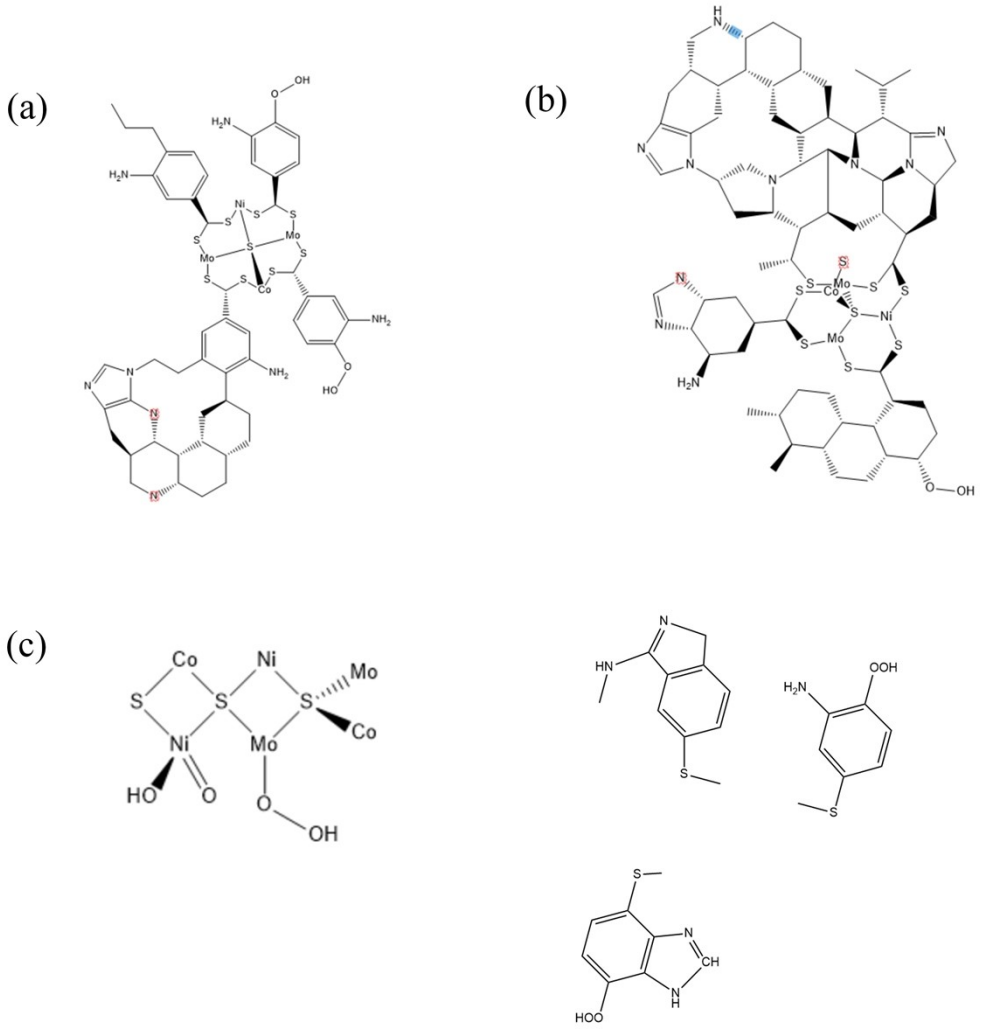


**Fig. S21.** Structural inference (taking a basic unit as an example). (a) MILN-based Co(z)-NiMoS, (b) after HER stability test, (c) after OER stability test.

**Table S1.** Ni, Mo and Co cation content level of MILN-based Co(z)-NiMoS electrodes calculated by ICP-MS.

| element | Sample element content $C_x$（mg/kg) | w% |
|---|---|---|
| Co | 7759.26 | 0.78% |
| Mo | 12097.80 | 1.21% |
| Ni | 796678.24 | 79.67% |

**Table S2.** Comparison of electrochemical performance for MILN-based Co(z)-NiMoS with other non-noble metal bifunctional electrocatalysts for water splitting (1.0 M KOH solution)

| **Catalysts** | **HER activity** | | **OER activity** | | **OWS activity** | | $C_{dl}$ | *References* |
|---|---|---|---|---|---|---|---|---|
| | **μ10 (mV)** | **Tafel slope (mV dec$^{-1}$)** | **μ10 (mV)** | **Tafel slope (mV dec$^{-1}$)** | **μ10 (V)** | **μ50 (V)** | | |
| **MILN-based Co(z)-NiMoS** | **169** | **71** | **170** | **33** | **1.466** | **1.75** | **17.4** | **This work** |
| **$Co_3O_4$@Mo-$Co_3S_4$-$Ni_3S_2$** | 116 | 97 | 295 | 98 | 1.62 | 1.85 | 21 | **1** |
| **defect-Ni-MOF** | 101 | 42.3 | 219 | 48.2 | 1.5 | 1.6 | 2.92 | **2** |
| **$CoNi_2S_4$/$Ni_3S_2$** | 171 | 88.6 | 243 | 28.1 | 1.65 | 1.85 | 35.1 | **3** |

| | | | | | | | | |
|---|---|---|---|---|---|---|---|---|
| **$Ni_xCo_{1-x}MoO_4$@Co $MoO_4$** | 51 | 63 | 180 | 43 | 1.46 | 1.65 | 4.5 | **4** |
| **{111} faceted $Ni_3S_2$** | 189 | 89.3 | 296 | 65.1 | 1.55 | - | 2.38 | **5** |
| **$Ni_3S_2/MoS_2$** | 78 | 62 | 260 | 59 | 1.53 | 1.69 | - | **6** |
| **0.4 Co:FePi** | 82.3 | 221 | 227 | 42.6 | 1.72 | 2.4 | - | **7** |

**Table S3.** Comparison of electrochemical performance for prepared catalysts for HER, OER and OWS (1.0 M KOH solution)

| **Overpotential** | **MILN-based Co(z)-NiMoS** | **Co(z)-NiMoS** | **MILN-based Co-NiMoS** | **Co-NiMoS** | **NiMoS** | **MIL-88B(Ni/Mo)-$NH_2$** |
|---|---|---|---|---|---|---|
| **HER μ10 (mV)** | **168** | **205** | **206** | **219** | **230** | **235** |
| **OER μ10 (mV)** | **170** | **205** | **207** | **220** | **234** | **239** |
| **OER μ50 (mV)** | **279** | **333** | **306** | **339** | **381** | **510** |
| **OER μ100 (mV)** | **399** | **447** | **482** | **478** | **602** | **656** |
| **OWS μ10 (V)** | **1.466** | **1.58** | **1.588** | **1.607** | **1.66** | **1.827** |

# References


1. Q. Wu, A. Dong, C. Yang, L. Ye, L. Zhao and Q. Jiang, *Chem. Eng. J*, 2020, **12**, 127482.
2. J. Zhou, Y. Dou, X. Q. Wu, A. Zhou, L. Shu and J. R. Li, *Small*, 2020, **16**, 1906564.
3. W. Dai, K. Ren, Y.-a. Zhu, Y. Pan, J. Yu and F. Lu, *J. Alloy. Compd.*, 2020, **844**, 156252.
4. Z. Li, M. Zheng, X. Zhao, J. Yang and W. Fan, *Nanoscale*, 2019, **11**, 22820-22831.
5. L. Li, C. Sun, B. Shang, Q. Li, J. Lei, N. Li and F. Pan, *Journal of Materials Chemistry A*, 2019, **7**, 18003-18011.
6. C. Wang, X. Shao, J. Pan, J. Hu and X. Xu, *Appl. Catal. B-environ*, 2020, **268**, 118435.
7. S. A. Khalate, S. A. Kadam, Y.-R. Ma, S. S. Pujari and U. M. Patil, *J. Alloys Compd.*, 2021, **885**, 160914.